Implementation of cold-formed steel stress-strain relationships using limited available material parameters

Junbo Chen[1], Zhiliang Chen[2], Haixin Liu[3,*], Tak-Ming Chan[4]

Abstract: Implementation of existing stress-strain models for cold-formed steels requires the input of key material parameters determined from corner coupon tests on cold-formed portions. The present paper proposes various approaches that can accurately describe the stress-strain responses of cold-formed steels by using corner material properties if known, or by using parent material properties and the corner geometry after cold-forming in the absence of corner material properties. A comprehensive database of coupon test results of cold-formed steels is firstly assembled. A total of 483 corner coupon test results with 236 full stress-strain curves are collected from 31 sources, covering a large range of steel grades with nominal yield strength varying from 235 MPa to 960 MPa. The applicability of existing empirical models for determination of the enhanced yield strength, ultimate strength and ultimate strain is carefully evaluated. New predictive expressions for the required input parameters, namely 0.01% or 0.05% proof stresses for the use of two-stage Ramberg-Osgood model, and the strain-hardening exponent for the use of one-stage material model are subsequently derived. Prediction performances of the two-stage Ramberg-Osgood model and the one-stage model are then evaluated against experimental stress-strain curves under different availability of primary material

[1] Associate Professor, School of Civil and Hydraulic Engineering, Huazhong University of Science and Technology, Wuhan, Hubei, China. Email: junbochen@hust.edu.cn

[2] Master Student, School of Civil and Hydraulic Engineering, Huazhong University of Science and Technology, Wuhan, Hubei, China. Email: zhiliangchen@hust.edu.cn

[3] Postdoctoral Fellow, Department of Civil and Environmental Engineering, The Hong Kong Polytechnic University, Hung Hom, Hong Kong, China. Email: hai-xin.liu@connect.polyu.hk (corresponding author)

[4] Professor, Department of Civil and Environmental Engineering, The Hong Kong Polytechnic University, Hung Hom, Hong Kong, China. Email: tak-ming.chan@polyu.edu.hk

parameters. According to the proposed approaches, the minimum required input parameters to utilize these models are only the yield strength of cold-formed steels or, alternatively, the yield strength of the parent metal and corner geometry after cold-forming. The developed models are proven to be accurate in predicting the monotonic stress-strain response (up to the ultimate point) of cold-formed steels, and are suitable for use in parametric studies and advanced modeling of cold-formed structures.

Keywords: Cold-formed steels; Stress-strain relationship; Ramberg-Osgood model; Strength enhancement; Material properties.

Introduction

Cold-formed steels, such as roll-formed hollow sections and press-braked open sections, have been widely used in constructions due to ease of prefabrication, economic efficiency of mass production, and high strength and stiffness-to-weight ratios (Gardner and Yun, 2018, Liu, Chen and Chan, 2023). Generally, cold-formed steels are characterized by a rounded stress-strain response with enhanced strengths but a loss of ductility due to the plastic deformation introduced during cold-forming (Gardner, Saari and Wang, 2010). Typical stress-strain curves of a steel plate before and after cold-forming are illustrated in Fig. 1. Commonly used cold-forming processes for cold-formed steel products include roll-forming and press-braking (Karren, 1967). During the cold-forming processes, plastic deformation is introduced. Different regions within the cross-sections undergo various levels of plastic deformation. As a result, the material properties of steels in deformed regions vary from those of parent materials due to the generated permanent deformation and random dislocation between crystal boundaries (Chajes, Britvec and Winter, 1963). Corner regions of cold-formed cross-

sections normally experience larger plastic deformations than cold-formed circular hollow sections due to their lower radius-to-thickness ratios, hence having higher yield and ultimate strengths.

Over the past few decades, a number of studies have been carried out to develop suitable models to predict the enhanced yield strength in corner regions. It was found that the enhancement of material strengths is related to material properties of parent metal and the amount of plastic deformation of cold-formed corners which can be reflected by the inner or outer radius-to-thickness ratio of the corners, r_i/t or r_o/t (Karren, 1967). Empirical predictive expressions have been proposed to determine the enhanced yield and ultimate strengths of cold-formed steels (Abdel-Rahman and Sivakumaran, 1997, Afshan, Rossi and Gardner, 2013, Gardner, Saari and Wang, 2010, Karren, 1967, Liu, Chen and Chan, 2023, Liu, Chen and Chan, 2024, Rossi, Afshan and Gardner, 2013), and standardized methods to calculate the strength enhancement in cold-formed steel sections have been incorporated in current design codes worldwide (AISI, 2016, CEN, 2006). Comprehensive literature reviews of existing strength enhancement models can be found elsewhere (Li, Yuan and Hong, 2023, Rossi, Afshan and Gardner, 2013).

With the increasing use of advanced numerical analyses in the design of steel structures, it has been observed that more accurate results can be generated in the numerical simulations when the corner properties are properly considered in the finite element models (Chen, Zhu and Chan, 2020, Gardner and Nethercot, 2004). It is therefore imperative to develop accurate and practical material models to describe the stress-strain responses of cold-formed steels. There exist some material models for cold-formed steels, such as the modified two-stage Ramberg-Osgood model (Gardner and Yun, 2018) and one-stage stress-strain relationship (Ma, Chan and Young, 2015). To use these stress-strain models, key material parameters are required, for example the 0.01% proof stress or 0.05% proof

stress for the two-stage Ramberg-Osgood model and the strain-hardening exponent for the one-stage model. It should be noted that the modified two-stage Ramberg-Osgood model (Gardner and Yun, 2018) has been standardized in prEN 1993-1-14 (CEN, 2023) for the generation of stress-strain curves of cold-formed steel and high strength steel. However, if the primary material parameters of cold-formed steels are not reported, where no measurements of corner properties are taken, the aforementioned models cannot be directly used due to the absence of required inputs. Therefore, predictive expressions for determinations of these required inputs for existing models are needed. Recently, comprehensive experimental investigations into the changes of material properties in cold-formed corner regions have been carried out in Liu, Chen, Chan (2023, 2024) and recommendations have been given to determine the Young's modulus, the enhanced strengths, the ultimate strain (i.e. the total strain corresponding to the ultimate strength) and etc. However, to accurately obtain the stress-strain curves of cold-formed steel, further predictive expressions, for example the 0.01% proof stress or 0.05% proof stress, are still needed. Moreover, to replicate the effect of cold-forming on parent materials, it is also of great interests to develop material models that can predict the stress-strain behaviors of cold-formed steels based on the material properties of parent metal and the amount of plastic deformation, without conduction of corner coupon tests, which is the focus of current study. With these developed models, it would be easier to carry out numerical parametric studies to investigate the structural behaviors of cold-formed members with varying corner radii, and it is also beneficial to developing finite element-based design methods of cold-formed members in practice.

This paper presents the developments of stress-strain models to describe the monotonic stress-strain responses (up to the ultimate point) of cold-formed steels. The existing material stress-strain relationships and predictive expressions for material properties of cold-formed steels are firstly

reviewed. A comprehensive experimental database of corner coupon tests is collated, which includes a total of 483 corner coupon test results from 31 sources. A large range of steel grades with nominal yield strength ranging from 235 MPa to 960 MPa, is covered in the assembled database. Based on the database, existing expressions for the enhanced yield strength, the enhanced ultimate strength and ultimate strain are assessed. Subsequently, predictive expressions for the required input parameters, namely 0.01% and 0.05% proof stresses for the use of two-stage Ramberg-Osgood model, and the strain-hardening exponent for one-stage material model, are derived. The predictions of stress-strain curves under different availability of primary material properties are then discussed and the predicted stress-strain curves are finally compared with experimental curves to examine the accuracy of the proposed models.

Overview and limitations of existing works

Stress-strain models for cold-formed steels

The rounded stress-strain responses of cold-formed carbon steels and stainless steels have been widely described by the Ramberg-Osgood model (Hill, 1944, Ramberg and Osgood, 1943), which is generally expressed using three basic parameters (see Eq. (1)), namely, the Young's modulus E, steel yield strength f_y (taken as the 0.2% proof stress $f_{0.2}$ for rounded stress-strain responses) and strain hardening exponent n. Hill (1944) proposed to use two offset strength values to simplify the original Ramberg-Osgood model. The widely used two offset strengths can be the yield strength f_y (0.2% proof stress $f_{0.2}$) and the 0.01% proof stress $f_{0.01}$ (also known as proportional limit), and the strain hardening exponent n can be then determined through Eq. (2). Recently, it was observed that replacing the 0.01% proof stress in Eq. (2) by 0.05% proof stress $f_{0.05}$ has shown to yield better predictions of

stainless steel and cold-formed carbon steel stress-strain curves (Arrayago, Real and Gardner, 2015, Gardner and Yun, 2018, Real*, et al.*, 2014). Hence, Eq. (3) can be used in place of Eq. (2).

$$\varepsilon = \frac{\sigma}{E} + 0.002\left(\frac{\sigma}{f_{0.2}}\right)^n \tag{1}$$

$$n = \frac{\ln(0.2 / 0.01)}{\ln(f_{0.2} / f_{0.01})} = \frac{\ln(20)}{\ln(f_{0.2} / f_{0.01})} \tag{2}$$

$$n = \frac{\ln(0.2 / 0.05)}{\ln(f_{0.2} / f_{0.05})} = \frac{\ln(4)}{\ln(f_{0.2} / f_{0.05})} \tag{3}$$

The original Ramberg-Osgood model was found to be generally incapable of accurately representing the full stress-strain curve of stainless steel with a single value of n. A smooth two-stage Ramberg-Osgood model was proposed in Mirambell and Real (2000) to represent the stress-strain curve: the conventional Ramberg-Osgood relationship was utilized up to the yield point in the first stage, while a modified Ramberg-Osgood model commencing at the yield point was used for the second stage. The second stage was obtained by moving both vertical and horizontal axes from the origin to the yield point of the stress-strain curve corresponding to the 0.2% proof stress. The modified two-stage model can be therefore expressed by Eq. (4), in which $E_{0.2}$ is the tangential modulus at 0.2% proof stress, f_u is the ultimate strength, $\varepsilon_{0.2}$ and ε_u are the total strains at yield and ultimate points, respectively, and m is the the strain hardening exponent at the second stage. Due to the continuity at the transition point, $E_{0.2}$ can be determined by Eq. (5).

$$\varepsilon = \begin{cases} \dfrac{\sigma}{E} + 0.002\left(\dfrac{\sigma}{f_{0.2}}\right)^n & \text{for } \sigma \le f_{0.2} \\ \dfrac{\sigma - f_{0.2}}{E_{0.2}} + \left(\varepsilon_u - \varepsilon_{0.2} - \dfrac{f_u - f_{0.2}}{E_{0.2}}\right)\left(\dfrac{\sigma - f_{0.2}}{f_u - f_{0.2}}\right)^m + \varepsilon_{0.2} & \text{for } \sigma > f_{0.2} \end{cases} \tag{4}$$

$$E_{0.2} = \frac{E}{1 + 0.002nE / f_{0.2}} \tag{5}$$

The two-stage Ramberg-Osgood model was further simplified by Rasmussen (2003) by

approximating the plastic strain term (ε_u - $\varepsilon_{0.2}$ - (σ - $f_{0.2}$)/$E_{0.2}$) to the ultimate strain ε_u. Use of the aforementioned models needs inputs of basic material parameters, like the first and second strain hardening exponents, n and m, yield and ultimate strength, $f_{0.2}$ and f_u, etc. To facilitate the use of the two-stage Ramberg-Osgood model, further recent investigations (Gardner and Yun, 2018) have been carried out to propose predictive expressions, applicable to cold-formed carbon steels, for the key parameters used in the two-stage Ramberg-Osgood model. Based on a large database of results with over 700 experimental stress-strain curves, Eqs. (6) and (7) have been proposed for the predictions of the second strain hardening exponent m and the ultimate strain ε_u, respectively. Normally, the 0.01% and 0.05% proof stresses for the determination of the first strain hardening exponent n are acquired from corner coupon tests. However, unlike the commonly used yield strength and ultimate strength, 0.01% and 0.05% proof stresses are not reported in some studies, resulting in the difficulty in determining the strain hardening exponent n.

$$m = 1 + 3.3\frac{f_{0.2}}{f_u} \tag{6}$$

$$\varepsilon_u = 0.6\left(1 - \frac{f_{0.2}}{f_u}\right) \tag{7}$$

Hradil *et al.* (2013) adopted the same idea of two-stage model and developed a generalized multistage model based on the Ramberg-Osgood expression. Ma, Chan and Young (2015) followed the concept of multiple segments and found that the strain-hardening exponent n for different segments decreases with the increase in plastic strain ε_p. A new strain-hardening exponent n_{ma} was then proposed as a continuous function of plastic strain, as expressed in Eq. (8), where n is the original strain-hardening exponent (Eqs. (2) and (3)), m_{ma} and K are the exponent and coefficient for calculating n_{ma}. Substituting Eq. (8) into Eq. (1), an explicit formula to determine stress-strain curves is presented in Eq. (9) or Eq. (10). This model can be therefore named as the one-stage model in this

paper.

$$n_{\mathrm{ma}} = f\left(\varepsilon_{\mathrm{p}}\right) = \frac{1}{n + K\varepsilon_{\mathrm{p}}^{m_{\mathrm{ma}}}} \tag{8}$$

$$\sigma = f_{0.2}\left(\frac{\varepsilon_{\mathrm{p}}}{0.002}\right)^{n_{\mathrm{ma}}} \tag{9}$$

$$\varepsilon = \varepsilon_{\mathrm{p}} + \frac{\sigma}{E} = \varepsilon_{\mathrm{p}} + \frac{f_{0.2}}{E}\left(\frac{\varepsilon_{\mathrm{p}}}{0.002}\right)^{n_{\mathrm{ma}}} \tag{10}$$

Substituting the ultimate strength f_{u} and plastic strain at ultimate point $\varepsilon_{\mathrm{pu}}$ (= ε_{u} - f_{u}/E) into Eq. (9), the coefficient K can be determined by Eq. (11). Stress-strain curves can be obtained using the one-stage model when the yield strength f_{y}, ultimate strength f_{u}, ultimate strain ε_{u}, original strain-hardening exponent n and the exponent m_{ma} are obtained. As shown in (Chen and Chan, 2020, Chen, Liu and Chan, 2020), the stress-strain curves predicted from this one-stage model correlate well with test results. However, it should be noted that the exponent m_{ma} was determined by fitting the model prediction to the test stress-strain data. If the coupon test results are not available, the exponent m_{ma} cannot be obtained directly. Predictive expressions to determine the exponent m_{ma} are therefore derived in this paper based on available material parameters, which will be detailed in the following section.

$$K = \left[\log_{f_{\mathrm{u}}/f_{0.2}}\left(\frac{\varepsilon_{\mathrm{u}} - f_{\mathrm{u}}/E}{0.002}\right)\right] / \left(\varepsilon_{\mathrm{u}} - f_{\mathrm{u}}/E\right)^{m_{\mathrm{ma}}} \tag{11}$$

Predictive expressions for strength enhancements

Early studies into the cold-forming effect on conventional steels were conducted by Karren (1967). Note that the measured yield strength of virgin materials used in Karren's study ranged from 212 MPa to 295 MPa. On the basis of power equation assumption and simplified corner analysis model, a predictive expression for enhanced yield strengths f_{yc} was derived, as formulated in Eqs. (12)

- (14). In these equations, f_{yc} and f_{yf} are the yield strengths of the cold-formed material and virgin material, respectively, f_{uf} is the ultimate strength of virgin material, r_i is the inner corner radius of the cold-formed material, and t is the material thickness. Letters "c" and "f" in the subscripts indicate cold-formed and virgin material, respectively. This model has been standardized in the North American Cold-Formed Steel Specification AISI S100-16 (AISI, 2016).

$$\frac{f_{yc}}{f_{yf}}=\frac{B_c}{(r_i/t)^m} \tag{12}$$

$$B_c = 3.69\frac{f_{uf}}{f_{yf}}\text{-}0.819\left(\frac{f_{uf}}{f_{yf}}\right)^2\text{-}1.79 \tag{13}$$

$$m = 0.192\frac{f_{uf}}{f_{yf}}\text{-}0.068 \tag{14}$$

It was observed by Abdel-Rahman and Sivakumaran (1997) that strength enhancements also exist in the flat-corner adjacent areas based on tensile coupon test results on cold-formed steel channel sections. To account for the nonhomogeneous material properties due to uneven levels of plastic deformation, an average enhanced yield strength within the corner zone, defined as the curved corner plus adjacent flat regions with an extended length of $\pi r_i/2$ on either side of the corner, was proposed, as given in Eq. (15). Based on a comparative experimental investigation, modifications to Karren's model, Eqs. (12) - (14), were also made by Gardner, Saari and Wang (2010) for roll-formed hollow sections. The revised enhanced yield strength model is given in Eq. (16).

$$\frac{f_{yc}}{f_{yf}}=0.6\left[\frac{3.69\left(f_{uf}/f_{yf}\right)\text{-}0.819\left(f_{uf}/f_{yf}\right)^2\text{-}1.79}{(r_i/t)^{0.192\left(f_{uf}/f_{yf}\right)-0.068}}-1\right]+1 \tag{15}$$

$$\frac{f_{yc}}{f_{yf}}=\frac{2.90\left(f_{uf}/f_{yf}\right)\text{-}0.752\left(f_{uf}/f_{yf}\right)^2\text{-}1.09}{(r_i/t)^{0.23\left(f_{uf}/f_{yf}\right)-0.041}} \tag{16}$$

More recently, Liu, Chen and Chan (2023, 2024) carried out extensive experimental investigations into the changed material properties in cold-formed regions. In the experimental

programs, a wide range of steel grades from Q235 to Q690 were included. Expressions for B_c and m in Eq. (12) were recalculated through regression analyses on the basis of a larger database of results, and the new proposed expression for the enhanced yield strength is presented in Eq. (17). Inspired by the expression of Eq. (17), a revised expression for the prediction of enhanced ultimate strength f_{uc} was also proposed, as given in Eq. (18), which adopted the same mathematical form as Eq. (17), but with different coefficients.

$$\frac{f_{yc}}{f_{yf}}=\frac{2.769\left(f_{uf}/f_{yf}\right)-0.581\left(f_{uf}/f_{yf}\right)^2-1.182}{\left(r_i/t\right)^{0.314\left(f_{uf}/f_{yf}\right)-0.320}} \tag{17}$$

$$\frac{f_{uc}}{f_{yf}}=\frac{2.807\left(f_{uf}/f_{yf}\right)-0.505\left(f_{uf}/f_{yf}\right)^2-1.217}{\left(r_i/t\right)^{0.254\left(f_{uf}/f_{yf}\right)-0.265}} \tag{18}$$

Experimental database of cold-formed steels

To characterize the material properties of cold-formed steels in corner regions, a total of 483 corner coupon test results from 31 sources (Afshan, Rossi and Gardner, 2013, Chen, Liu and Chan, 2020, Fang, Chan and Young, 2018, Gardner, Saari and Wang, 2010, Guo*, et al.*, 2007, Jiang and Zhao, 2022, Jiang and Zhao, 2022, Key, Hasan and Hancock, 1988, Kyvelou, Gardner and Nethercot, 2017, Li and Young, 2022, Liu, Chen and Chan, 2023, Liu, Chen and Chan, 2024, Liu*, et al.*, 2022, Liu, Fang and Chan, 2022, Liu, Fang and Chan, 2022, Liu*, et al.*, 2022, Ma, Chan and Young, 2015, Pandey and Young, 2019, Somodi and Kövesdi, 2017, Tayyebi and Sun, 2020, Wang, Zhao and Young, 2019, Wang, Zhao and Young, 2020, Wang*, et al.*, 2017, Wilkinson and Hancock, 1998, Xiao, 2021, Yang*, et al.*, 2022, Zhang*, et al.*, 2019, Zhang*, et al.*, 2020, Zhong*, et al.*, 2021, Zhu, Chan and Young, 2019) are collected to establish a comprehensive database. It should be noted that some unpublished test data from authors' research group are also included in the database. And different fabrication

methods, i.e. press-braking and cold-rolling, are included in the database. In terms of coupons extracted from cold-rolled sections, results of flat coupons machined from the flat face are used to represent material properties of parent materials. This approach is acceptable since the average strength enhancement of flat materials in cold-rolled hollow sections was only around 4% (Gardner, Saari and Wang, 2010). The assembled database covers a large range of steel grades with nominal yield strength of parent steels varying from 235 MPa to 960 MPa. The thickness t of steels and the inner radius to thickness ratio r_i/t ranges from 0.74 mm to 9.94 mm, and 0.52 to 7.54, respectively. Table 1 summarizes the key information of the coupon test database, including steel grade (or yield strength), available numbers of data points for basic material parameters, such as the Young's modulus E_c, 0.01% proof stress $f_{0.01c}$, 0.05% proof stress $f_{0.05c}$, yield strength f_{yc} (or 0.2% proof stress $f_{0.2c}$), ultimate tensile strength f_{uc}, ultimate strain ε_{uc}, and inner corner radius to thickness ratio r_i/t. Among the 483 corner coupon test results in the database, a total of 236 full stress-strain curves are collected. It should be noted that the collected 236 full stress-strain curves are reanalyzed to determine the 0.01% and 0.05% proof stresses of each curve.

The collated test results will be firstly used to assess the existing predictive expressions for the enhanced yield strength, the enhanced ultimate strength, and the ultimate strain. Predictive expressions for the 0.01% proof stress $f_{0.01c}$, 0.05% proof stress $f_{0.05c}$, and the exponent m_{ma}, will be derived as well based on the collated database. As shown in Table 1, 236 data points are used in the derivation of the predictive expression for the 0.01% proof stress $f_{0.01c}$, 236 for the 0.05% proof stress $f_{0.05c}$, 483 for the enhanced yield strength f_{yc}, 479 for the enhanced ultimate strength f_{uc}, 388 for the ultimate strain ε_{uc}, and 236 for m_{ma}, respectively.

Analysis of results and recommendations

The use of existing material stress-strain relationships for cold-formed steels, such as the modified two-stage Ramberg-Osgood model (Gardner and Yun, 2018, Mirambell and Real, 2000, Rasmussen, 2003) and one-stage model (Ma, Chan and Young, 2015), needs the input of basic material properties of cold-formed corners, including the Young's modulus E_c, yield strength f_{yc}, ultimate strength f_{uc}, and ultimate strain ε_{uc}, etc. These basic material properties of cold-formed steels can be determined through corner coupon tests. Without some of these values (for example the exponent m_{ma} for the one-stage model), these existing material models cannot be directly used to regenerate the full stress-strain curves. In this section, existing predictive expressions for the enhanced yield strength f_{yc}, enhanced ultimate strength f_{uc} and ultimate strain ε_{uc} are firstly assessed. Further predictive expressions are developed for the 0.01% proof stress $f_{0.01c}$, 0.05% proof stress $f_{0.05c}$ to be used in the two-stage model and the exponent m_{ma} in one-stage model (see Eqs. (8) - (10)). With these expressions, these material parameters can be calculated without the conduction of corner coupon tests.

Enhanced yield strength f_{yc}

For the prediction of enhanced yield strength f_{yc} of cold-formed steels, various semi-empirical models have been derived, like Karren model (Karren, 1967) (Eqs. (12) - (14)), Abdel-Rahman and Sivakumaran model (Abdel-Rahman and Sivakumaran, 1997) (Eq. (15)), Gardner model (Gardner, Saari and Wang, 2010) (Eq. (16)), Liu model (Liu, Chen and Chan, 2023, Liu, Chen and Chan, 2024) (Eq. (17)), and among others. As presented in Table 1, 483 data points are available for evaluating the accuracy of these models. Assessment of these four models for the prediction of f_{yc} is presented in

Fig. 2, in which the predicted values $f_{yc,pred}$ are plotted with regard to the measured values $f_{yc,test}$. Table 2 summarizes statistical results concerning the mean prediction-to-test $f_{yc,pred}/f_{yc,test}$ values and corresponding coefficient of variations (CoVs). As indicated in Fig. 2 and Table 2, Liu model yields considerably more accurate and less scattered predictions of f_{yc} than other models, with the mean prediction-to-test value of 0.997 (closest to unity) and the smallest CoV of 0.068. It is worth noting that benefiting from a larger database of corner coupon test results, Liu model (Liu, Chen and Chan, 2023, 2024) is more universally applicable to a wider range of steel grades. It is therefore recommended that Eq. (17) can be used for the determination of enhanced yield strength f_{yc} of cold-formed steels.

Enhanced ultimate strength f_{uc}

In this section, a total of 479 data points collated in the database are used to assess existing models for the prediction of enhanced ultimate strength f_{uc} of cold-formed steels. In previous studies (Fukumoto, 1996, Gardner and Yun, 2018, Langenberg, 2008), empirical relationships between f_{uc}/f_{yc} and f_{yc} were proposed, as given by Eqs. (19) - (21), respectively. By utilizing these equations, the enhanced ultimate strength f_{uc} can be predicted based on the enhanced yield strength f_{yc}. Otherwise, if the corner material properties are unknown, Eq. (18) can be adopted to predict the enhanced ultimate strength f_{uc} based on the material properties of parent metal, f_{yf} and f_{uf}, and corner geometry after cold-forming r_i/t. Eq. (18) was originally proposed for normal strength steels in Liu, Chen and Chan (2023), and then extended to predict the enhancement of ultimate strength for high strength steels up to 960 MPa by Liu, Chen and Chan (2024).

$$f_{uc}/f_{yc} = 1+\left(130/f_{yc}\right)^{1.4} \tag{19}$$

$$f_{uc}/f_{yc} = 0.83 + 203.8/f_{yc} \tag{20}$$

$$f_{uc}/f_{yc} = \left[1 - 0.72e^{\left(-0.0027 f_{yc}\right)}\right]^{-1} \tag{21}$$

The accuracy of Eqs. (18) - (21) has been further evaluated herein against the collated test results, as shown in Fig. 3, in which the predictions of ultimate strength $f_{uc,pred}$ are plotted against the corresponding test values $f_{uc,test}$. Statistical results of the evaluation concerning the mean prediction-to-test $f_{uc,pred}/f_{uc,test}$ values and corresponding CoVs are summarized in Table 3. As illustrated in Fig. 3 and Table 3, predictions from Eqs. (19) and (18) show better agreements with experimental results when compared to the other two models, with mean prediction-to-test $f_{uc,pred}/f_{uc,test}$ values of 1.011 and 0.997, and corresponding CoVs of 0.052 and 0.070, respectively. Therefore, Eq. (19) can be used to predict the ultimate strength f_{uc} of cold-formed steels in instances where the yield strength f_{yc} is known, while Eq. (18) can be used when f_{yf}, f_{uf}, and r_i/t are reported in the absence of the yield strength f_{yc}.

Ultimate strain ε_{uc}

In terms of the prediction of ultimate strain ε_{uc} for cold-formed steels, Eqs. (22) - (23) have been proposed by Gardner and Yun (2018) and Liu, Chen and Chan (2024), respectively. The collected 388 data points are used to evaluate the accuracy of the two expressions for the determination of ε_{uc}. Evaluation results are depicted in Fig. 4, in which the predictions of ultimate strain $\varepsilon_{uc,pred}$ are plotted with regard to corresponding test values $\varepsilon_{uc,test}$. It can be seen from Fig. 4 that Gardner and Yun model (Gardner and Yun, 2018) tends to overestimate the ultimate strain ε_{uc}, yielding a mean prediction-to-test $\varepsilon_{uc,pred}/\varepsilon_{uc,test}$ value and corresponding CoV of 2.721 and 0.362, respectively, while Liu model (Liu, Chen and Chan, 2024) slightly underestimates ε_{uc}, giving a mean prediction-to-test $\varepsilon_{uc,pred}/\varepsilon_{uc,test}$ value of 0.912 and a moderate corresponding CoV of 0.397. Therefore, Eq. (23) can be used to predict the

ultimate strain ε_{uc} of cold-formed steel with slight underestimation.

$$\varepsilon_{uc} = 0.6\left(1 - f_{yc}/f_{uc}\right) \tag{22}$$

$$\varepsilon_{uc} = 0.01\left(f_{uc}/f_{yc}\right)^{\left(28 f_{uc}/f_{yc} - 25.4\right)} \tag{23}$$

0.01% and 0.05% proof stresses $f_{0.01c}$ and $f_{0.05c}$

To make use of the two-stage Ramberg-Osgood model (see Eq. (4)), the first strain hardening exponent n is a necessary input parameter. The exponent n can be calculated using classic expressions, as given in Eqs. (2) and (3), where 0.01% and 0.05% proof stresses of cold-formed steels, $f_{0.01c}$ and $f_{0.05c}$, are required, respectively. Therefore, it is of great interests to propose predictive expressions to compute $f_{0.01c}$ and $f_{0.05c}$.

If the enhanced yield strength f_{yc} is available, inspired by the expression of Eq. (19), $f_{0.01c}/f_{yc}$ and $f_{0.05c}/f_{yc}$ are firstly plotted against f_{yc} in Fig. 5. Revised expressions for predictions of $f_{0.01c}$ and $f_{0.05c}$ are then proposed, as given in Eqs. (24) and (25), respectively. These equations adopt the same mathematical form as Eq. (19), but with different coefficients. If the yield strength of parent metal f_{yf} and the corner geometry r_i/t are available, following the same regression analysis approaches as f_{yc} and f_{uc} (Eqs. (17) and (18)), revised expressions for $f_{0.01c}$ and $f_{0.05c}$ are proposed as well as shown in Eqs. (26) and (27). In the regression analyses, 236 and 236 data points are used for $f_{0.01c}$ and $f_{0.05c}$, respectively.

$$\frac{f_{0.01c}}{f_{yc}} = 0.589 + \left(\frac{225.5}{f_{yc}}\right)^{3.7} \tag{24}$$

$$\frac{f_{0.05c}}{f_{yc}} = 0.808 + \left(\frac{205}{f_{yc}}\right)^{4.0} \tag{25}$$

$$\frac{f_{0.01c}}{f_{yf}} = \frac{2.366\left(f_{uf}/f_{yf}\right) - 0.692\left(f_{uf}/f_{yf}\right)^2 - 1.019}{\left(r_i/t\right)^{-0.224\left(f_{uf}/f_{yf}\right) + 0.343}} \tag{26}$$

$$\frac{f_{0.05c}}{f_{yf}} = \frac{3.087\left(f_{uf}/f_{yf}\right)\text{-}0.878\left(f_{uf}/f_{yf}\right)^2\text{-}1.336}{\left(r_i/t\right)^{0.104\left(f_{uf}/f_{yf}\right)-0.060}} \tag{27}$$

Assessments of Eqs. (24) - (27) for the determination of $f_{0.01c}$ and $f_{0.05c}$ are presented in Figs. 6 and 7, where the predicted values $f_{0.01c,pred}$ and $f_{0.05c,pred}$ are plotted with respect to the corresponding test values $f_{0.01c,test}$ and $f_{0.05c,test}$, respectively. As demonstrated by Figs. 6 and 7, Eqs. (24) - (27) produce comparatively accurate predictions. And the mean prediction-to-test values of $f_{0.01c,pred}/f_{0.01c,test}$ are 1.004 and 0.998, with corresponding CoVs of 0.069 and 0.105, and the mean prediction-to-test values of $f_{0.05c,pred}/f_{0.05c,test}$ are 1.001 and 1.004, with corresponding CoVs of 0.032 and 0.073, respectively. It can be observed from the assessment results that the predictions of $f_{0.05c}$ from Eqs. (25) and (27) are more accurate and less scattered than those of $f_{0.01c}$. In the prediction of the first strain hardening exponent n in the two-stage Ramberg-Osgood model, two alternatives can be used, as given in Eqs. (2) and (3). It is found that Eq. (3) gives better predictions of exponent n and therefore generates better predictions of cold-formed steel stress-strain curves. Hence, Eq. (3) is recommended to determine the exponent n. Similar recommendations have been given elsewhere in Gardner and Yun (2018) and prEN 1993-1-14 (CEN, 2023). Therefore, Eqs. (3) combined with (25) can be used to predict the exponent n when the yield strength of cold-formed corner f_{yc} is known, while Eqs. (3) combined with (27) can be used when f_{yf}, f_{uf}, and r_i/t are reported in the absence of the f_{yc}.

Exponent m_{ma} in one-stage model

The use of the one-stage model (Ma, Chan and Young, 2015) requires the input of exponent m_{ma}. Regression analyses are firstly conducted on the collated 236 corner coupon stress-strain curves to obtain the fitted m_{ma} value of each curve. In view of different availability of primary material properties, two predictive equations are proposed accordingly. If the corner material properties were

given, the m_{ma} value could be predicted by a formula of the enhanced yield strength f_{yc} and ultimate strength f_{uc}. If the corner material properties were unknown, the material properties of parent metal, f_{yf} and f_{uf}, and the corner geometry after cold-forming r_i/t may be used to predict the exponent m_{ma}.

Based on careful evaluations on these two scenarios, it is found that the exponent m_{ma} can be expressed as functions of f_{yc}/f_{uc} and $(r_i/t)\times\ln(f_{uf}/f_{yf})$, respectively. On the basis of further nonlinear regression analyses, predictive expressions for the exponent m_{ma} can be given by Eqs. (28) and (29). The data points of fitted exponent m_{ma} plotted with fitting curves, as well as the 95% confidence and prediction bands are presented in Figs. 8 and 9. The mean predicted-to-fitted values of m_{ma} are equal to 0.998 and 1.027, with corresponding CoVs of 0.359 and 0.282, respectively.

$$m_{ma} = 2.179 \cdot \exp(f_{yc} / f_{uc}) - 4.742 \tag{28}$$

$$m_{ma} = \exp(-0.781 \cdot (r_i / t) \ln(f_{uf} / f_{yf})) \tag{29}$$

Proposed stress-strain models for cold-formed steels

To accurately describe the stress-strain behaviors of cold-formed steels, various approaches are proposed in this section. The modified two-stage Ramberg-Osgood model (Gardner and Yun, 2018) and one-stage model (Ma, Chan and Young, 2015) for cold-formed steels are adopted, but with proposed predictive expressions for input parameters detailed in section "Analysis of results and recommendations". In view of different availability of primary material properties, two scenarios are considered herein. Firstly, when corner material properties are available, different methods to generate stress-strain curves are discussed in the sub-section "Scenario 1: Corner material properties available". In the following sub-section "Scenario 2: Corner material properties unavailable", the second scenario is assumed that corner material properties are unavailable, and the curves are

generated based on the material properties of parent metal, f_{yf} and f_{uf}, and corner geometry after cold-forming r_i/t. The accuracy of the proposed approaches is evaluated through comparisons of representative predicted stress-strain curves with corresponding experimental curves from the collected database. Six representative corner coupon test results, covering a wide range of steel grades as summarized in Table 4, are used for evaluation.

Scenario 1: Corner material properties available

If the corner material properties are available, it may be assumed that the measured Young's modulus E_c, yield strength f_{yc}, ultimate strength f_{uc}, ultimate strain ε_{uc}, strain hardening exponents n and m for the two-stage model, and the exponent m_{ma} for the one-stage model are reported in various degrees of completeness. Considering different availability of the key input parameters, three cases for Scenario 1 are discussed herein, as summarized in Table 5, and the accuracy of each case is graphically assessed.

In Case 1, it is assumed that the measured material parameters E_c, f_{yc}, f_{uc}, ε_{uc}, n, m, and m_{ma} are known. The six representative specimens, as reported in Table 4, are used to assess the accuracy of the proposed models. Comparisons of these predicted curves with experimental curves are presented in Figs. 10(a), 11(a), 12(a), 13(a), 14(a), and 15(a). Both the two-stage and one-stage models produce accurate stress-strain curve predictions. It is noteworthy that as compared with the two-stage model, the one-stage model exhibits exceptional accuracy in capturing the stress-strain response from the yield point to the ultimate point, highlighting its effectiveness in predicting stress-strain curves for cold-formed steels.

In Case 2, it is assumed that the basic material properties E_c, f_{yc}, and f_{uc} are known. In this case,

suitable existing expressions are adopted to predict the unavailable input parameters. $f_{0.05c}$ is determined from Eq. (25), ε_{uc} is predicted using Eq. (23), the strain hardening exponent n is calculated from Eq. (3), the strain hardening exponent m is predicted using Eq. (6), and the exponent m_{ma} for the one-stage model is predicted using Eq. (28). The predicted values in Case 2 are listed in Table 6. Comparisons of the predicted curves in Case 2 with the experimental curves are shown in Figs. 10(b), 11(b), 12(b), 13(b), 14(b), and 15(b). Both the two-stage and one-stage models are able to produce accurate stress-strain curve predictions, though small discrepancies can be observed in ε_{uc}.

In Case 3, it is assumed that only f_{yc} is known. E_c is taken as the recommended value of 197 GPa (Liu, Chen and Chan, 2024) , f_{uc} and ε_{uc} are predicted using Eqs. (19) and (23), $f_{0.05c}$ is determined from Eq. (25), n is predicted using Eq. (3), m and m_{ma} are predicted using Eqs. (6) and (28) based on the predicted f_{uc}, respectively. The predicted values in Case 3 are presented in Table 6. Figs. 10(c), 11(c), 12(c), 13(c), 14(c), and 15(c) depict the comparisons of the predicted curves in Case 3 with the experimental curves. Due to the limited availability of measured material properties, the two-stage and one-stage models are still capable of generating acceptable stress-strain curve predictions, though the accuracy of the predicted stress-strain curves decreases.

Scenario 2: Corner material properties unavailable

The focus of this section is to propose stress-strain relationships that can predict the stress-strain responses of cold-formed steels when the corner material properties are unavailable. By using the proposed approaches, stress-strain curves of cold-formed steels can be predicted based on the material properties of parent metal E_f, f_{yf}, f_{uf}, and the corner geometry r_i/t. It is important to emphasize that in Scenario 2, the availability of r_i/t is crucial. Without it, the effect of cold-forming cannot be evaluated,

and consequently, stress-strain curves cannot be obtained. Similar to Scenario 1, two cases (Case 4 and 5, numbered sequentially following the section "Scenario 1: Corner Material Properties Available") are considered in Scenario 2, as summarized in Table 7, based on the availability of key input parameters, and the following approaches are recommended.

In Case 4, it is assumed that the measured material parameters E_f, f_{yf}, f_{uf}, and corner geometry r_i/t are known. Material properties of cold-formed steels, namely, $f_{0.01c}$, $f_{0.05c}$, f_{yc}, f_{uc}, are firstly determined from Eqs. (26), (27), (17), (18), respectively. E_c can be taken as $0.95E_f$ or the recommended value of 197 GPa. Alternatively, $f_{0.01c}$ and $f_{0.05c}$ can be calculated from Eqs. (24) and (25) using the predicted f_{yc}. Based on the predicted corner material strengths, ε_{uc} is then predicted using Eq. (23), the strain hardening exponent n is calculated from Eq. (3), the strain hardening exponent m is predicted using Eq. (6), and the exponent m_{ma} for the one-stage model is predicted using Eq. (28). It should be noted that Eq. (29) can be adopted to predict m_{ma} as well if f_{yf}, f_{uf} and r_i/t are given. The predicted values in Case 4 are presented in Table 8. Figs. 16(a), 17(a), 18(a), 19(a), 20(a), and 21(a) show the comparisons of the predicted curves in Case 4 with the experimental curves. The comparison results indicate that predictions using the proposed approaches consistently match well with the experimental stress-strain curves.

In Case 5, it is assumed that only measured f_{yf} and r_i/t are available. In this case, a predictive equation proposed by Gardner and Yun (2018), as given in Eq. (30), is firstly used to determine the ultimate strength f_{uf} and the recommended value of 197 GPa is assigned to E_c. Subsequently, material parameters $f_{0.01c}$, $f_{0.05c}$, f_{yc}, f_{uc}, ε_{uc}, n, m, and m_{ma} can be obtained following the same approaches as Case 4. The predicted values in Case 5 are presented in Table 8 and the comparisons of the predicted curves with the experimental curves are demonstrated in Figs. 16(b), 17(b), 18(b), 19(b), 20(b), and

21(b). Due to the unavailability of some material parameters, the proposed models generate acceptable but less accurate stress-strain predictions since some empirical expressions are used to calculate the input parameters.

$$f_{uf}/f_{yf}=1+\left(200/f_{yf}\right)^{1.75} \tag{30}$$

As can be observed from the evaluations of different cases in Figs. 10-21, the accuracy of the predicted stress-strain curves depends on the availability of key input parameters. The more material parameters are known, the more accurate predictions can be obtained. It should be noted that the minimum required input parameters are the yield strength of cold-formed steels f_{yc} for Scenario 1, and the yield strength of parent metal f_{yf} and corner radius-to-thickness ratio r_i/t for Scenario 2. Based on the comparison results, it can be concluded that the developed models are proven to be accurate in predicting the stress-strain response of cold-formed steels, and are suitable for use in parametric studies and advanced modeling of cold-formed structures.

Conclusion

A comprehensive investigation into the monotonic stress-strain relationships of cold-formed steels has been carried out in the present study. First of all, the existing material models to describe the stress-strain curves of cold-formed steels and investigations into the effect of cold work of forming are reviewed. Predictive expressions for the enhanced yield strength, ultimate strength and ultimate strain in existing literature are then evaluated based on a large database collated in this study. New predictive expressions for the 0.01% and 0.05% proof stresses and the strain-hardening exponent m_{ma}, which are the required key inputs for the two-stage Ramberg-Osgood model and the one-stage model, are derived as well. Various approaches are recommended to generate stress-strain curves under

different availabilities of material parameters. A total of five cases with different material properties availability are considered and discussed. Under different scenarios, the minimum required inputs can be only the yield strength of corner portions, or the yield strength of parent metal and radius-to-thickness ratio of deformed corners. More accurate predictions are generated when more reported key material parameters are input into the material models. It is shown that the stress-strain curves predicted using the proposed approaches agree satisfactorily with test results. The proposed models are proven to be appropriate to be used in numerical parametric studies and designs of cold-formed steels.

Supplementary materials

An automatic stress-strain curve generator for cold-formed steels, developed based on the proposed models in this paper, is available for free download at: https://www.researchgate.net/publication/377985367_Cold-formed_steel_stress-strain_curve_generator.

Acknowledgements

The research work presented in this paper was supported by the National Key R&D Program of China (2022YFC3801901) and the Research Grants Council of the Hong Kong Special Administrative Region, China (Project No. 15217119). Financial support from Chinese National Engineering Research Centre for Steel Construction (Hong Kong Branch) was also greatly appreciated. The authors would like to thank Dr. Xiang Yun from the University of Sheffield for sharing the experimental results.

Data Availability Statement

Some or all data, models, or code that support the findings of this study are available from the corresponding author upon reasonable request.

References

Abdel-Rahman, N., and Sivakumaran, K. (1997). "Material properties models for analysis of cold-formed steel members." *Journal of Structural Engineering*, 123(9), 1135-1143.

Afshan, S., Rossi, B., and Gardner, L. (2013). "Strength enhancements in cold-formed structural sections — Part I: Material testing." *Journal of Constructional Steel Research*, 83, 177-188.

AISI (2016). "AISI S100-16. North American Specification for the Design of Cold-Formed Steel Structural Members." American Iron and Steel Institute, The United States.

Arrayago, I., Real, E., and Gardner, L. (2015). "Description of stress–strain curves for stainless steel alloys." *Materials & Design*, 87, 540-552.

CEN (2006). "Eurocode 3 - Design of steel structures - Part 1-3: General rules - Supplementary rules for cold-formed members and sheeting." *EN 1993-1-3*, European Committee for Standardization (CEN), Brussels, Belgium.

CEN (2023). "Eurocode 3 - Design of steel structures - Part 1-14: Design assisted by finite element analysis." *prEN 1993-1-14*, European Committee for Standardization (CEN), Brussels, Belgium.

Chajes, A., Britvec, S., and Winter, G. (1963). "Effects of cold-straining on structural sheet steels." *Journal of the Structural Division*, 89(2), 1-32.

Chen, J., and Chan, T.-M. (2020). "Material properties and residual stresses of cold-formed high-strength-steel circular hollow sections." *Journal of Constructional Steel Research*, 170, 106099.

Chen, J., Liu, H., and Chan, T.-M. (2020). "Material properties and residual stresses of cold-formed octagonal hollow sections." *Journal of Constructional Steel Research*, 170, 106078.

Chen, J., Zhu, J.-Y., and Chan, T.-M. (2020). "Experimental and numerical investigation on stub column behaviour of cold-formed octagonal hollow sections." *Engineering Structures*, 214, 110669.

Fang, H., Chan, T.-M., and Young, B. (2018). "Material properties and residual stresses of octagonal high strength steel hollow sections." *Journal of Constructional Steel Research*, 148, 479-490.

Fukumoto, Y. (1996). "New constructional steels and structural stability." *Engineering Structures*, 18(10), 786-791.

Gardner, L., and Nethercot, D. A. (2004). "Numerical Modeling of Stainless Steel Structural Components—A Consistent Approach." *Journal of Structural Engineering*, 130(10), 1586-1601.

Gardner, L., Saari, N., and Wang, F. (2010). "Comparative experimental study of hot-rolled and cold-formed rectangular hollow sections." *Thin-Walled Structures*, 48(7), 495-507.

Gardner, L., and Yun, X. (2018). "Description of stress-strain curves for cold-formed steels." *Construction and Building Materials*, 189, 527-538.

Guo, Y.-J., Zhu, A.-Z., Pi, Y.-L., and Tin-Loi, F. (2007). "Experimental study on compressive strengths of thick-walled cold-formed sections." *Journal of Constructional Steel Research*, 63(5), 718-723.

Hill, H. (1944). "Determination of stress-strain relations from" offset" yield strength values." *Technical Note No. 927*, National Advisory committee for Aeronautics, Washington, D.C., USA.

Hradil, P., Talja, A., Real, E., Mirambell, E., and Rossi, B. (2013). "Generalized multistage mechanical model for nonlinear metallic materials." *Thin-walled structures*, 63, 63-69.

Jiang, K., and Zhao, O. (2022). "Net Section Failure of S690 High-Strength Steel Angle-to-Plate Connections." *Journal of Structural Engineering*, 148(4), 04022021.

Jiang, K., and Zhao, O. (2022). "Testing, numerical modelling and design of S690 high strength steel channel-to-plate connections." *Thin-Walled Structures*, 179.

Karren, K. W. (1967). "Corner properties of cold-formed steel shapes." *Journal of Structural Division*, 93(ST1, February), 401-432.

Key, P. W., Hasan, S. W., and Hancock, G. J. (1988). "Column behavior of cold-formed hollow sections." *Journal of Structural Engineering*, 114(2), 390-407.

Kyvelou, P., Gardner, L., and Nethercot, D. A. (2017). "Testing and Analysis of Composite Cold-Formed Steel and Wood−Based Flooring Systems." *Journal of Structural Engineering*, 143(11), 04017146.

Langenberg, P. (2008). "Relation between design safety and Y/T ratio in application of welded high strength structural steels." *International Symposium on Applications of High Strength Steels in*

*Modern Constructions and Bridges - Relationship of Design Specifications, Safety and Y/T Ratio*Beijing, China, 28-46.

Li, C.-L., Yuan, H., and Hong, H.-P. (2023). "Predicting yield strength of cold-formed carbon steel: A review and new approaches." *Journal of Constructional Steel Research*, 206.

Li, Q.-Y., and Young, B. (2022). "Experimental and numerical investigation on cold-formed steel built-up section pin-ended columns." *Thin-Walled Structures*, 170.

Liu, H., Chen, J., and Chan, T.-M. (2023). "Predictive models for material properties of cold-formed conventional steels in the corner region." *Thin-Walled Structures*, 187.

Liu, H., Chen, J., and Chan, T. M. (2024). "Mechanical properties of corner material in cold-formed steel structure: From normal strength to high strength." *Structures*, 59.

Liu, H., Jiang, H., Hu, Y.-F., Chan, T.-M., and Chung, K.-F. (2022). "Structural behaviour of Q355 and Q460 press-braked rectangular hollow section stub columns." *Journal of Constructional Steel Research*, 197, 107497.

Liu, J.-z., Fang, H., and Chan, T.-M. (2022). "Experimental and numerical investigations on stub column behaviour of cold-formed high strength steel irregular octagonal hollow sections." *Thin-Walled Structures*, 180.

Liu, J.-z., Fang, H., and Chan, T.-M. (2022). "Experimental investigations on material properties and stub column behaviour of high strength steel irregular hexagonal hollow sections." *Journal of Constructional Steel Research*, 196.

Liu, J.-z., Fang, H., Chen, S., and Chan, T.-M. (2022). "Material properties and residual stresses of high strength steel hexagonal hollow sections." *Journal of Constructional Steel Research*, 190.

Ma, J.-L., Chan, T.-M., and Young, B. (2015). "Material properties and residual stresses of cold-formed high strength steel hollow sections." *Journal of Constructional Steel Research*, 109, 152-165.

Mirambell, E., and Real, E. (2000). "On the calculation of deflections in structural stainless steel beams: an experimental and numerical investigation." *Journal of Constructional Steel Research*, 54, 109-133.

Pandey, M., and Young, B. (2019). "Tests of cold-formed high strength steel tubular T-joints." *Thin-Walled Structures*, 143, 106200.

Ramberg, W., and Osgood, W. R. (1943). "Description of stress-strain curves by three parameters."

Technical Note No. 902, National Advisory committee for Aeronautics, Washington, D.C., USA.

Rasmussen, K. J. R. (2003). "Full-range stress-strain curves for stainless steel alloys." *Journal of Constructional Steel Research*, 59, 47-61.

Real, E., Arrayago, I., Mirambell, E., and Westeel, R. (2014). "Comparative study of analytical expressions for the modelling of stainless steel behaviour." *Thin-Walled Structures*, 83, 2-11.

Rossi, B., Afshan, S., and Gardner, L. (2013). "Strength enhancements in cold-formed structural sections — Part II: Predictive models." *Journal of Constructional Steel Research*, 83, 189-196.

Somodi, B., and Kövesdi, B. (2017). "Flexural buckling resistance of cold-formed HSS hollow section members." *Journal of Constructional Steel Research*, 128, 179-192.

Tayyebi, K., and Sun, M. (2020). "Stub column behaviour of heat-treated and galvanized RHS manufactured by different methods." *Journal of Constructional Steel Research*, 166, 105910.

Wang, F., Zhao, O., and Young, B. (2019). "Flexural behaviour and strengths of press-braked S960 ultra-high strength steel channel section beams." *Engineering Structures*, 200.

Wang, F., Zhao, O., and Young, B. (2020). "Testing and numerical modelling of S960 ultra-high strength steel angle and channel section stub columns." *Engineering Structures*, 204.

Wang, J., Afshan, S., Schillo, N., Theofanous, M., Feldmann, M., and Gardner, L. (2017). "Material properties and compressive local buckling response of high strength steel square and rectangular hollow sections." *Engineering Structures*, 130, 297-315.

Wilkinson, T., and Hancock, G. J. (1998). "Tests to examine compact web slenderness of cold-formed RHS." *Journal of Structural Engineering*, 124(10), 1166-1174.

Xiao, M. (2021). "Structural behaviour of high strength S690 cold-formed square hollow sections under compression." Doctor of Philosophy Ph.D Thesis, The Hong Kong Polytechnic University.

Yang, L., Yin, F., Wang, J., Bilal, A., Ahmed, A. H., and Lin, M. (2022). "Local buckling resistances of cold-formed high-strength steel SHS and RHS with varying corner radius." *Thin-Walled Structures*, 172.

Zhang, L., Wang, F., Liang, Y., and Zhao, O. (2019). "Press-braked S690 high strength steel equal-leg angle and plain channel section stub columns: Testing, numerical simulation and design." *Engineering Structures*, 201.

Zhang, L., Wang, F., Liang, Y., and Zhao, O. (2020). "Experimental and numerical studies of press-braked S690 high strength steel channel section beams." *Thin-Walled Structures*, 148.

Zhong, Y., Sun, Y., Hai Tan, K., and Zhao, O. (2021). "Testing, modelling and design of high strength concrete-filled high strength steel tube (HCFHST) stub columns under combined compression and bending." *Engineering Structures*, 241.

Zhu, J.-Y., Chan, T.-M., and Young, B. (2019). "Cross-sectional capacity of octagonal tubular steel stub columns under uniaxial compression." *Engineering Structures*, 184, 480-494.

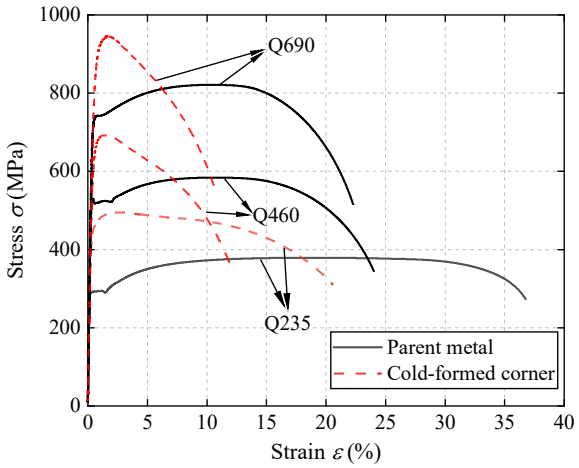

Fig. 1. Typical stress-strain curves before and after cold-forming.

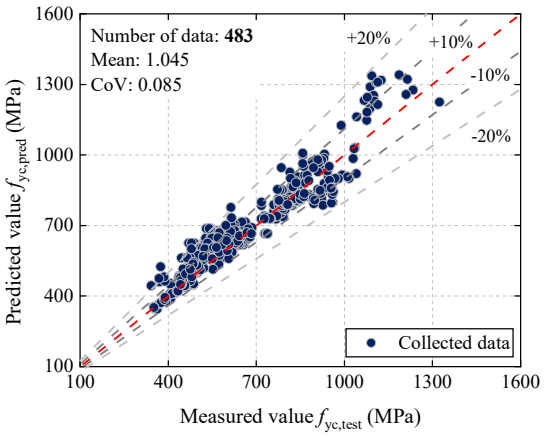

(a) Karren model (Karren, 1967)

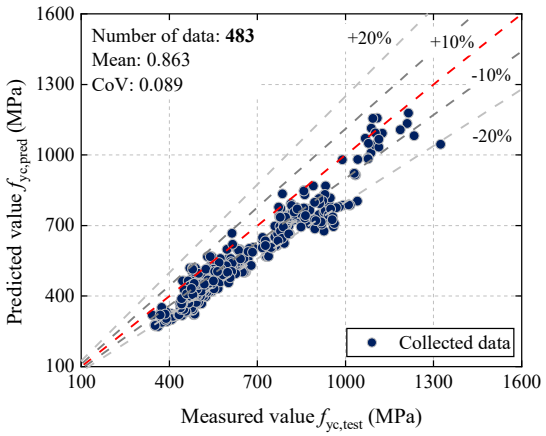

(b) Abdel-Rahman and Sivakumaran model (Abdel-Rahman and Sivakumaran, 1997)

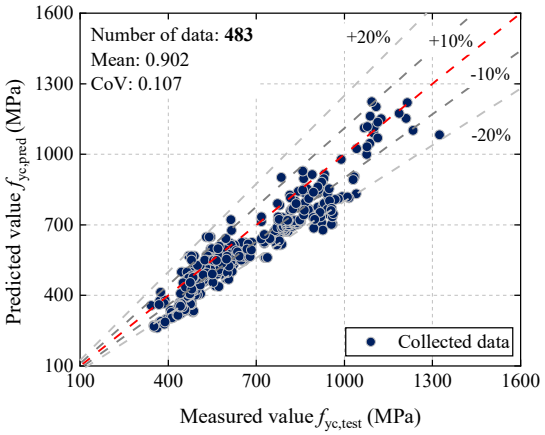

(c) Gardner model (Gardner, Saari and Wang, 2010)

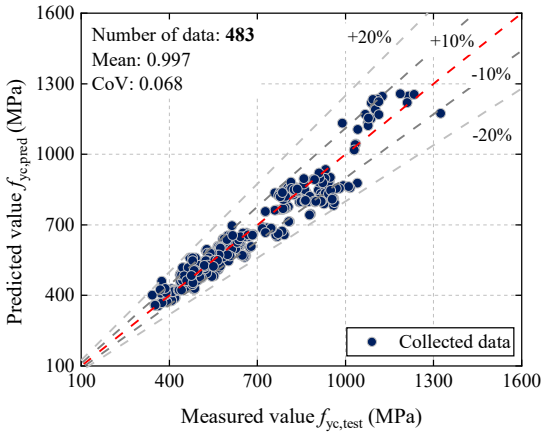

(d) Liu model (Liu, Chen and Chan, 2023, 2024)

Fig. 2. Assessment of existing models for enhanced yield strength f_{yc} of cold-formed steels.

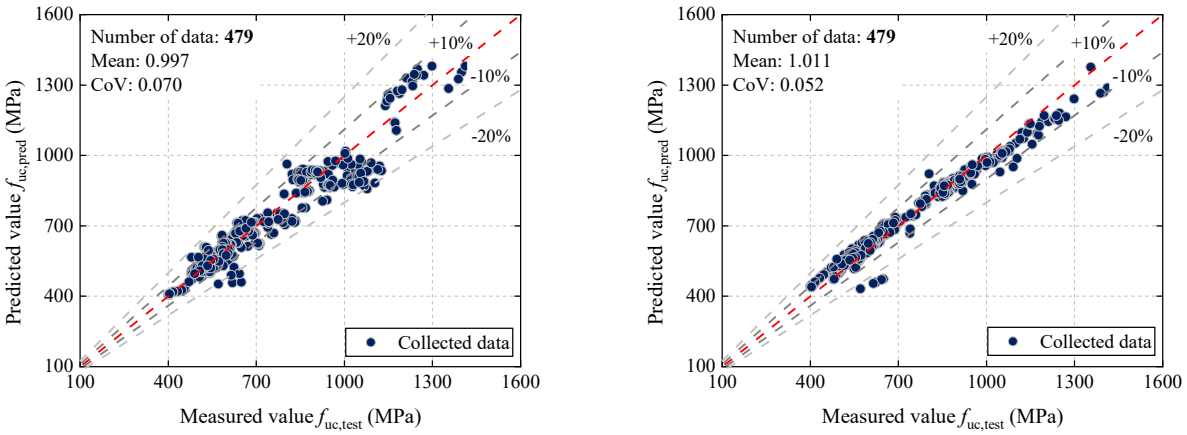

(a) Liu model (Liu, Chen and Chan, 2023, 2024)

(b) Gardner and Yun model (Gardner and Yun, 2018)

(c) Langenberg model (Langenberg, 2008)

(d) Fukumoto model (Fukumoto, 1996)

Fig. 3. Assessment of existing models for enhanced ultimate strength f_{uc} of cold-formed steels.

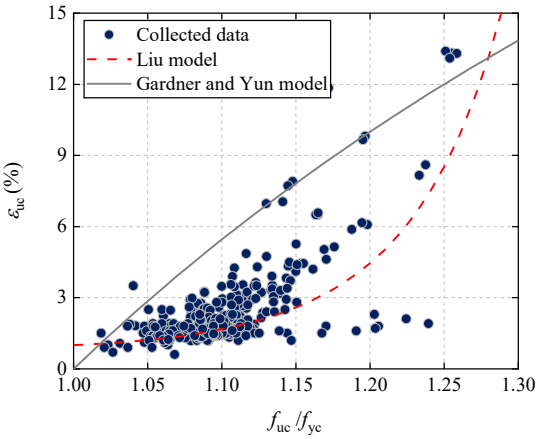

Fig. 4. Assessment of expressions for determination of ultimate strain ε_{uc}.

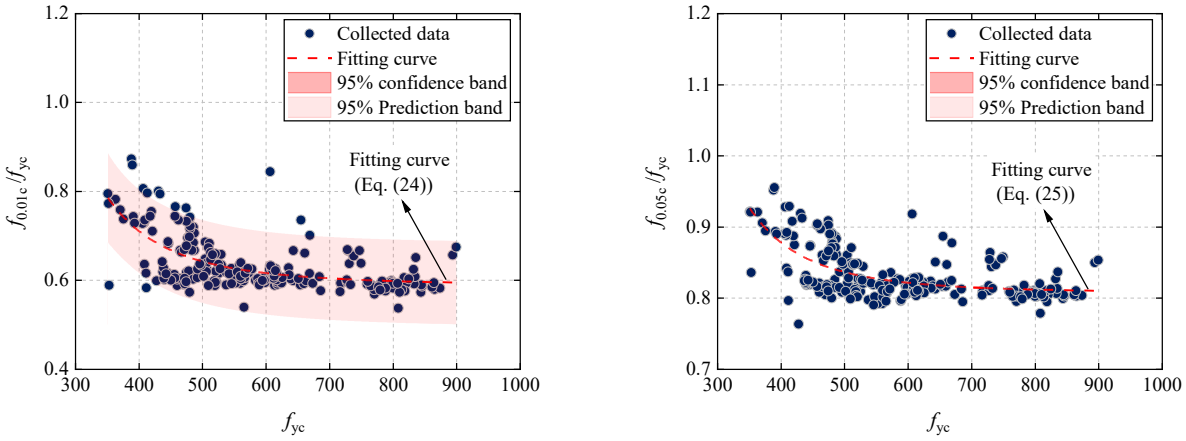

(a) 0.01% proof stress (b) 0.05% proof stress

Fig. 5. Trends of $f_{0.01c}/f_{yc}$ and $f_{0.05c}/f_{yc}$ against f_{yc}.

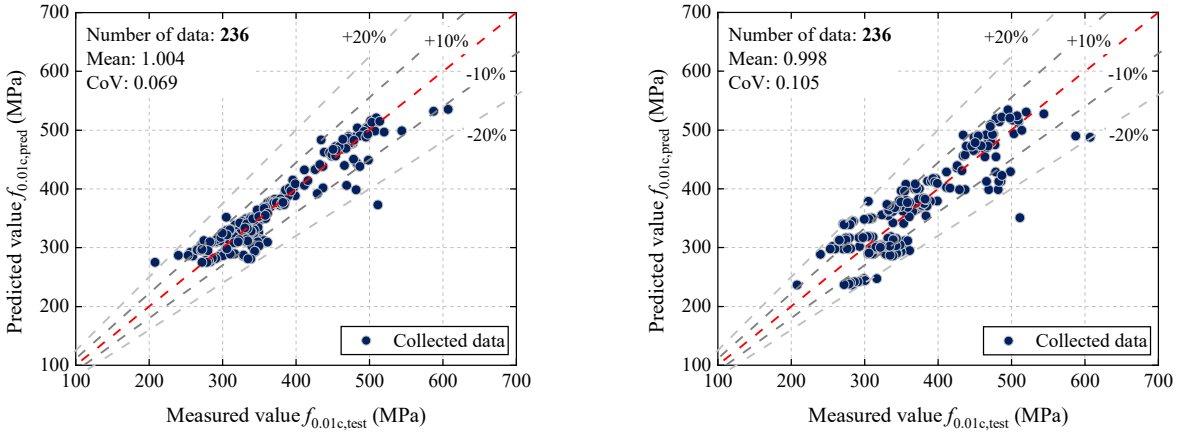

(a) Eq. (24) (b) Eq. (26)

Fig. 6. Assessment of expressions for determination of 0.01% proof stress $f_{0.01c}$.

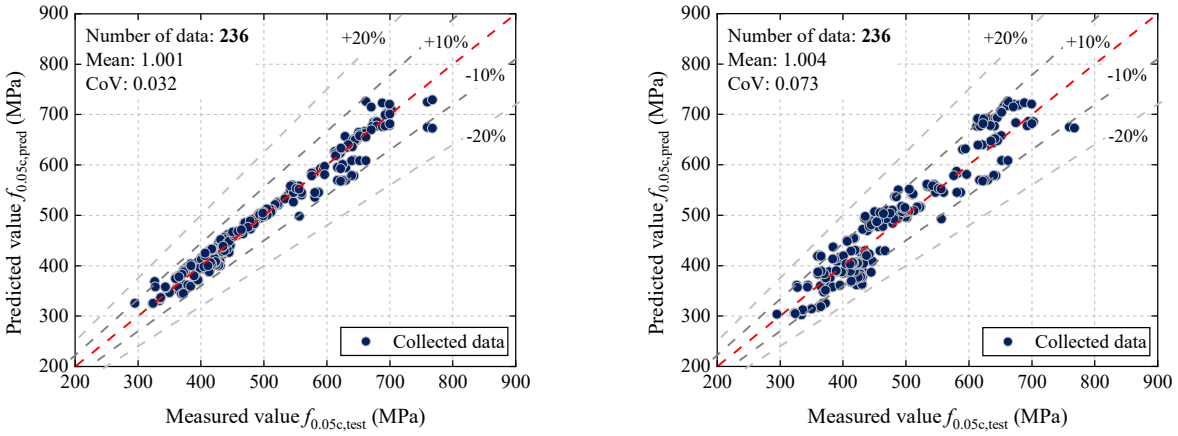

(a) Eq. (25) (b) Eq. (27)

Fig. 7. Assessment of expressions for determination of 0.05% proof stress $f_{0.05c}$.

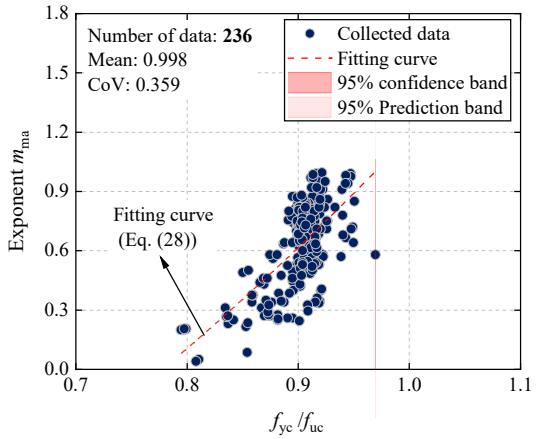

Fig. 8. Trend between fitted exponent m_{ma} and f_{yc}/f_{uc}.

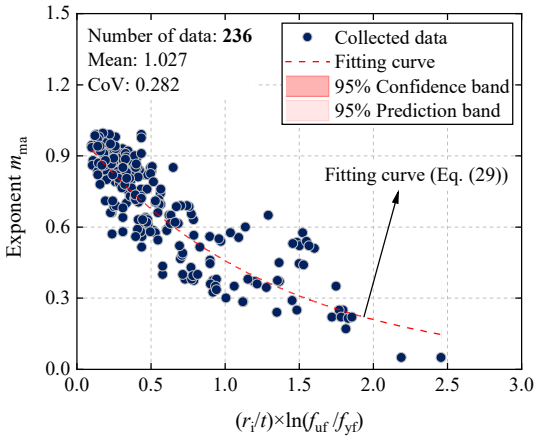

Fig. 9. Trend between fitted exponent m_{ma} and $(r_i/t)\times\ln(f_{uf}/f_{yf})$.

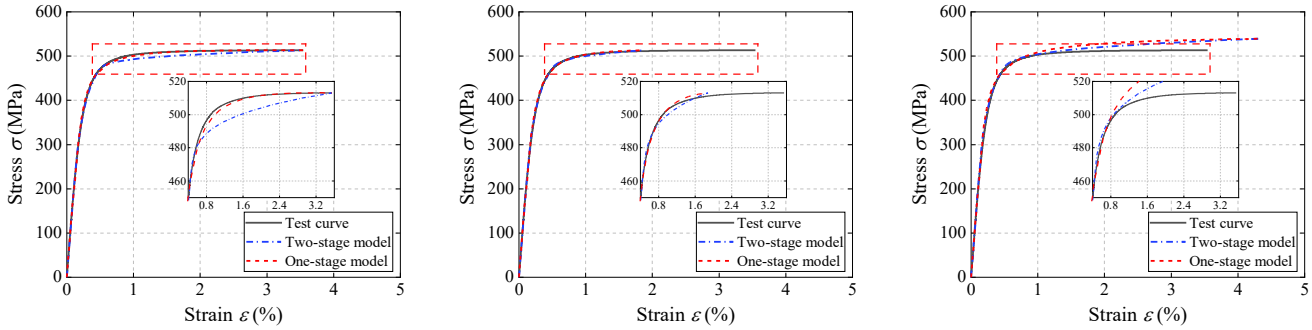

(a) Case 1 (b) Case 2 (c) Case 3

Fig. 10. Comparisons of predicted stress-strain curves in Scenario 1 with the test curve of 235-5-90-10-3 (Q235).

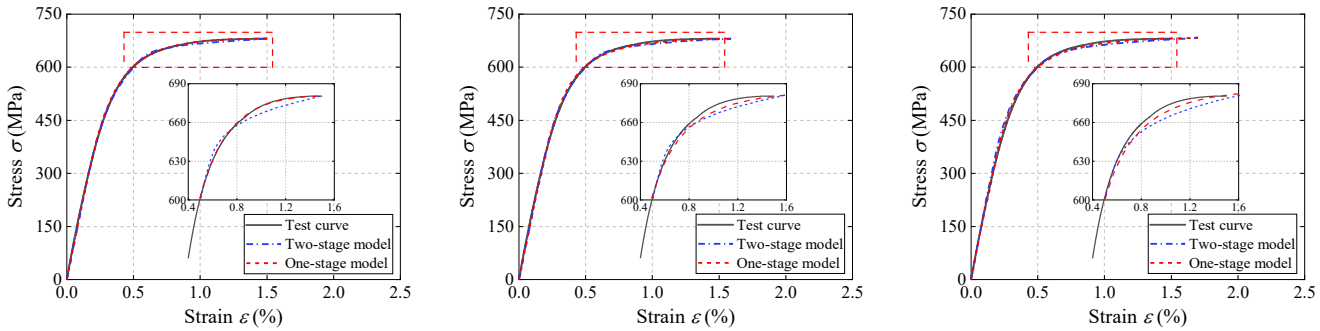

(a) Case 1 (b) Case 2 (c) Case 3

Fig. 11. Comparisons of predicted stress-strain curves in Scenario 1 with the test curve of 355-5cR-90-3-1 (Q355).

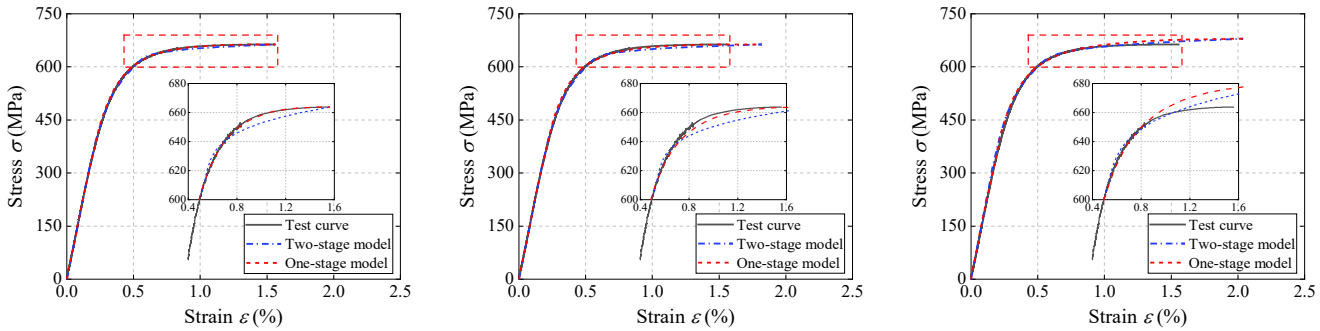

(a) Case 1 (b) Case 2 (c) Case 3

Fig. 12. Comparisons of predicted stress-strain curves in Scenario 1 with the test curve of 460-3-120-P5-2 (Q460).

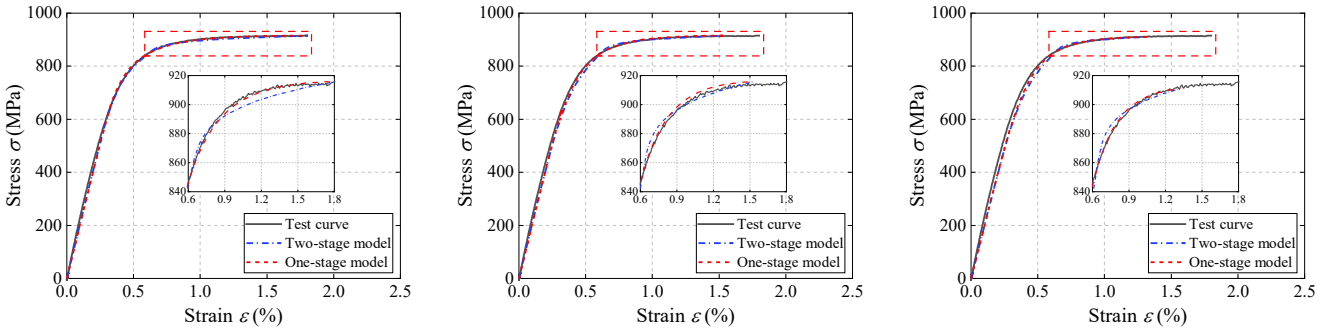

(a) Case 1 (b) Case 2 (c) Case 3

Fig. 13. Comparisons of predicted stress-strain curves in Scenario 1 with the test curve of CS-B4 (Q690).

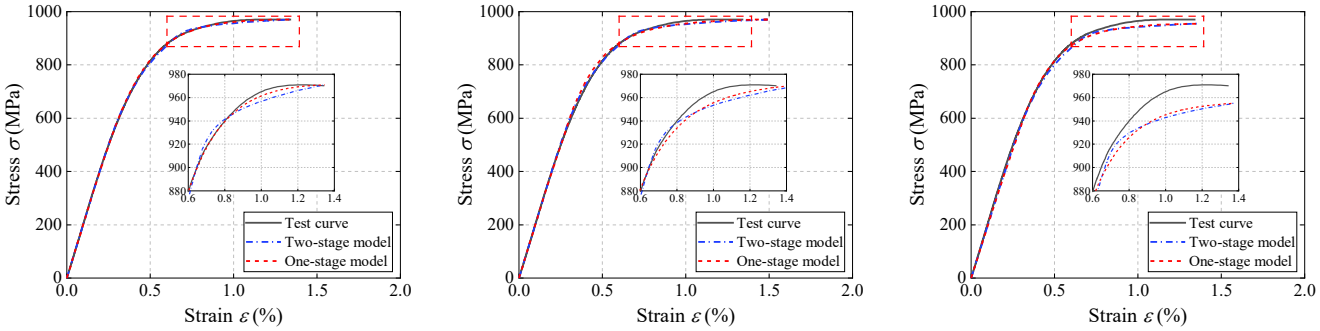

(a) Case 1 (b) Case 2 (c) Case 3

Fig. 14. Comparisons of predicted stress-strain curves in Scenario 1 with the test curve of H200×120×5 (S700).

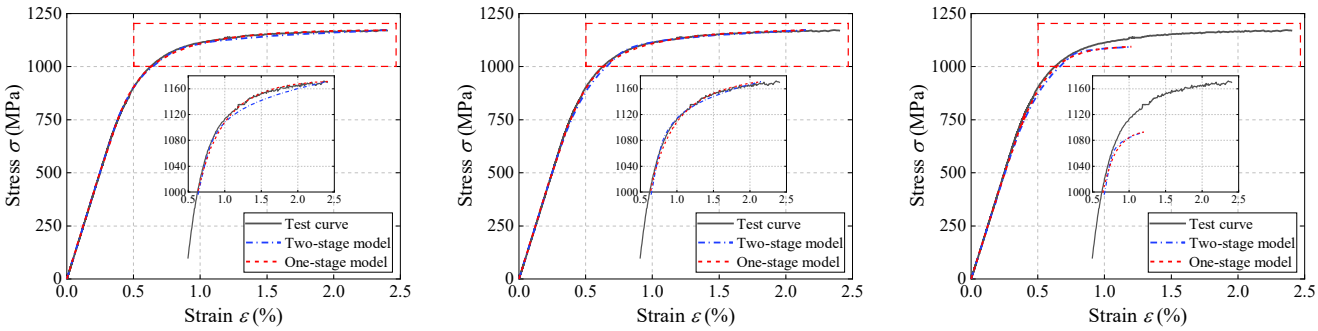

(a) Case 1 (b) Case 2 (c) Case 3

Fig. 15. Comparisons of predicted stress-strain curves in Scenario 1 with the test curve of A60×6-C (S960).

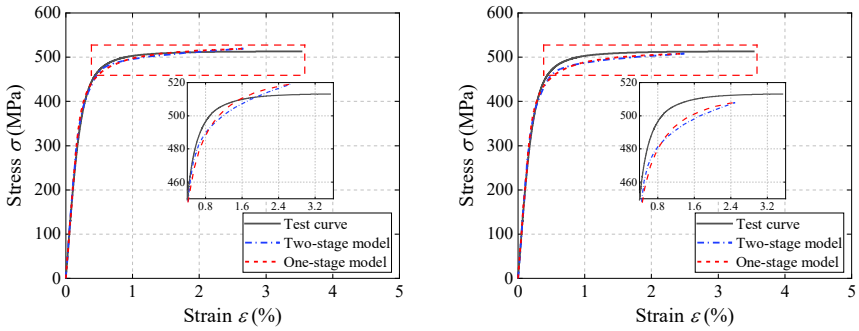

(a) Case 4 (b) Case 5

Fig. 16. Comparisons of predicted stress-strain curves in Scenario 2 with the test curve of 235-5-90-10-3 (Q235).

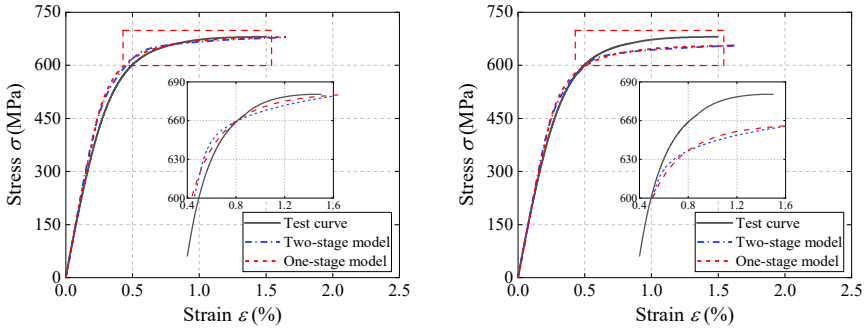

(a) Case 4 (b) Case 5

Fig. 17. Comparisons of predicted stress-strain curves in Scenario 2 with the test curve of 355-5cR-90-3-1 (Q355).

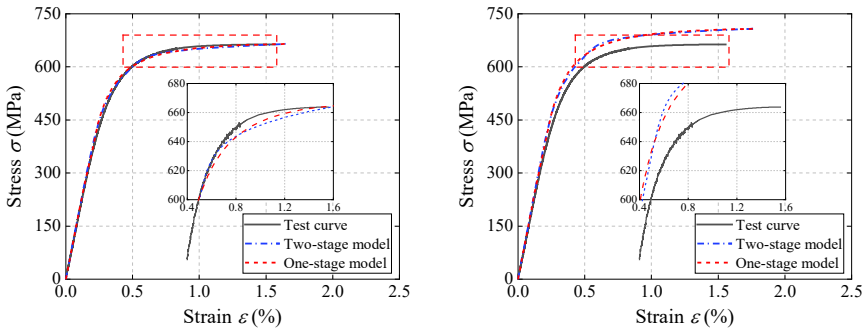

(a) Case 4 (b) Case 5

Fig. 18. Comparisons of predicted stress-strain curves in Scenario 2 with the test curve of 460-3-120-P5-2 (Q460).

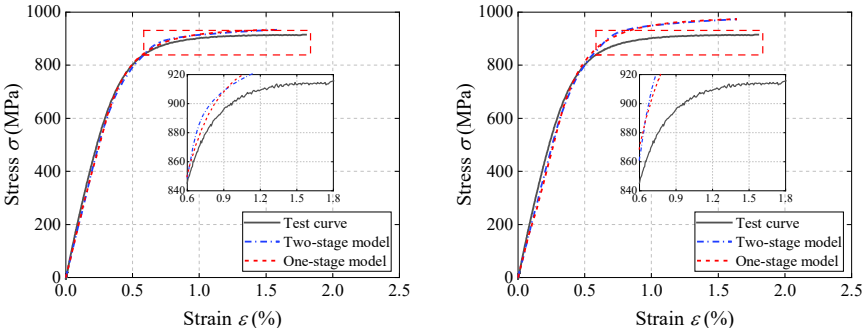

(a) Case 4 (b) Case 5

Fig. 19. Comparisons of predicted stress-strain curves in Scenario 2 with the test curve of CS-B4 (Q690).

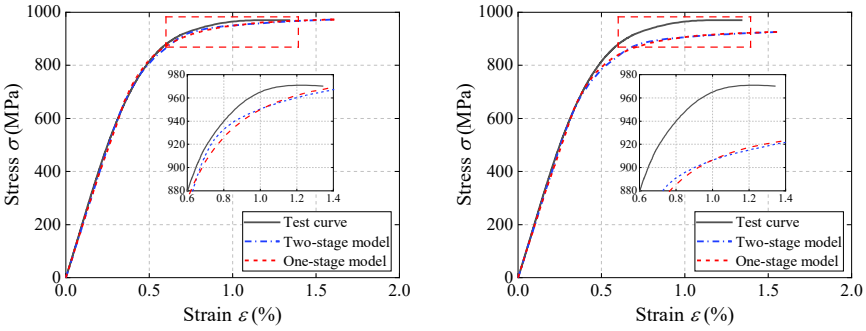

(a) Case 4 (b) Case 5

Fig. 20. Comparisons of predicted stress-strain curves in Scenario 2 with the test curve of H200×120×5 (S700).

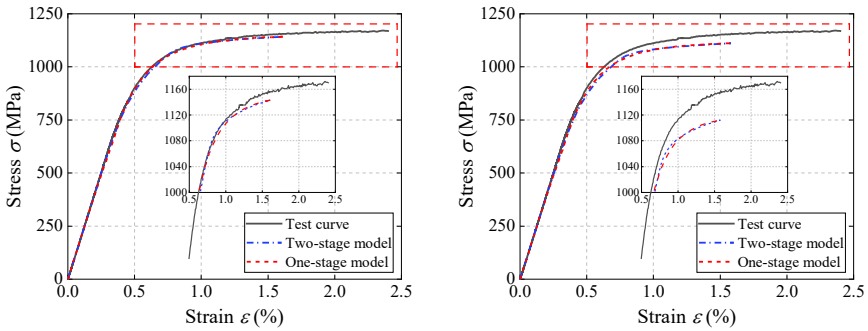

(a) Case 4 (b) Case 5

Fig. 21. Comparisons of predicted stress-strain curves in Scenario 2 with the test curve of A60×6-C (S960).

Table 1. Information summary of cold-formed steel material test data.

References	Steel grades or yield strengths	Fabrication & Sections	No. of data (Corner coupons)									
			E_c	$f_{0.01c}$	$f_{0.05c}$	f_{yc}	f_{uc}	ε_{uc}	ε_{fc}	r_i/t	m_{ma}	Full curve
Liu, Chen and Chan (2024)	Q460/Q550/Q690	Braked, Angle	66	66	66	66	66	66	66	66	66	66
Liu, Chen and Chan (2023)	Q235/Q275/Q355	Braked, Angle	143	143	143	143	143	143	143	143	143	143
Liu *et al.* (2022)	Q355/Q460	Braked, SHS/RHS	16	0	0	16	16	16	11	16	0	0
Li and Young (2022)	500 MPa/550 MPa	Built-up cold-formed sections	6	0	0	6	6	0	6	6	0	0
Liu, Fang and Chan (2022)	Q690	Braked, Hexagonal hollow sections	7	0	0	7	7	7	0	7	0	0
Liu, Fang and Chan (2022)	Q690	Braked, Hexagonal hollow sections	30	0	0	30	30	30	0	30	0	0
Liu *et al*. (2022)	Q690	Braked, Octagonal hollow sections	10	0	0	10	10	10	0	10	0	0
Jiang and Zhao (2022)	S690	Braked, Angle	4	0	0	4	4	4	0	4	0	0
Jiang and Zhao (2022)	S690	Braked, Channel sections	5	0	0	5	5	5	0	5	0	0
Xiao (Xiao, 2021)	S690	Braked, SHS	6	0	0	6	6	6	0	6	0	0
Yang *et al.* (2022)	S700/S900	Rolled, SHS	0	0	0	3	3	3	0	3	0	0
Zhong *et al.* (2021)	S700	Braked, SHS	4	0	0	4	4	4	0	4	0	0
Chen, Liu and Chan (2020)	460 MPa	Braked, Octagonal hollow sections	8	8	8	8	8	8	8	8	8	8
Tayyebi and Sun (2020)	344–730 MPa	Direct-formed or indirect-formed, RHS	10	0	0	10	10	0	0	10	0	0
Zhang *et al.* (2020)	S690	Braked, Channel sections	12	0	0	12	12	12	0	12	0	0
Wang, Zhao and Young (2020)	S960	Braked, Angle/channel	2	0	0	2	2	2	0	2	0	0
Pandey and Young (2019)	900 MPa/960 MPa	Rolled, SHS/RHS	10	0	0	10	10	0	0	10	0	0
Wang, Zhao and Young (2019)	S960	Braked, Channel sections	2	0	0	2	2	2	0	2	0	0
Zhang *et al.* (2019)	S690	Braked, Angle sections	6	0	0	6	6	6	0	6	0	0
Zhu, Chan and Young (2019)	355 MPa	Braked, SHS/RHS	2	0	0	2	2	2	0	2	0	0
Fang, Chan and Young (2018)	S690	Braked, Octagonal hollow sections	6	0	0	6	6	6	0	6	0	0
Kyvelou, Gardner and Nethercot (2017)	S450	Rolled, Channel sections	0	0	0	2	0	0	0	2	0	0
Somodi and Kovesdi (2017)	S700/S960	Rolled, SHS	0	0	0	3	3	0	0	3	0	0
Wang *et al.* (2017)	S500/S700/S960	Rolled, SHS	0	0	0	9	9	9	0	9	0	0
Ma, Chan and Young (2015)	S700/S900	Rolled, SHS/RHS	11	0	0	11	11	11	11	11	0	0
Afshan, Rossi and Gardner (2013)	S355	Rolled, SHS/RHS	8	0	0	8	6	6	0	8	0	0
Gardner, Saari, Wang (2010)	235 MPa	Rolled, SHS/RHS	5	0	0	5	5	0	5	5	0	0
Guo *et al.* (2007)	235 MPa	Rolled, SHS/RHS	0	0	0	6	6	0	0	6	0	0
Wilkinson and Hancock (1998)	C350/C450	Rolled, SHS/RHS	0	0	0	51	51	0	0	51	0	0
Key, Hasan and Hancock (1988)	350 MPa	Rolled, SHS/RHS	0	0	0	11	11	11	0	11	0	0
Unpublished data from authors	Q460/Q690	-	19	19	19	19	19	19	0	19	19	19
	Total		398	236	236	483	479	388	250	483	236	236

Table 2. Statistical results of $f_{yc,pred}/f_{yc,test}$ using different models.

Model	$f_{yc,pred}$ / $f_{yc,test}$			
	Karren model (Karren, 1967) Eqs. (12) - (14)	Abdel-Rahman and Sivakumaran model (Abdel-Rahman and Sivakumaran, 1997) Eq. (15)	Gardner model (Gardner, Saari and Wang, 2010) Eq. (16)	Liu model (Liu, Chen and Chan, 2023, 2024) Eq. (17)
Mean	1.045	0.863	0.902	0.997
CoV	0.085	0.107	0.107	0.068

Table 3. Statistical results of $f_{uc,pred}/f_{uc,test}$ using different models.

Model	$f_{uc,pred}$ / $f_{uc,test}$			
	Liu model (Liu, Chen and Chan, 2023, 2024) Eq. (18)	Gardner and Yun model (Gardner and Yun, 2018) Eq. (19)	Langenberg model (Langenberg, 2008) Eq. (20)	Fukumoto model (Fukumoto, 1996) Eq. (21)
Mean	0.997	1.011	1.051	1.052
CoV	0.070	0.052	0.071	0.078

Table 4. Representative cold-formed steel specimens used for comparisons.

Ref.	Steel grade	Specimen	E_f /GPa	f_{yf} /MPa	f_{uf} /MPa	r_i/t -	E_c /GPa	$f_{0.01c}$ /MPa	$f_{0.05c}$ /MPa	f_{yc} /MPa	f_{uc} /MPa	ε_{uc} /%	n -	m -	m_{ma} -
Liu, Chen and Chan (2023)	Q235	235-5-90-10-3	211	304	464	2.31	190	271	372	460	513	3.55	6.5	4.0	0.500
	Q355	355-5cR-90-3-1	215	431	559	0.96	185	373	492	613	681	1.50	6.3	4.0	0.875
Liu, Chen and Chan (2024)	Q460	460-3-120-P5-2	204	520	585	2.39	187	376	503	610	664	1.56	7.1	4.0	0.840
Xiao (2021)	Q690	CS-B4	217	795	837	3.06	206	638	672	850	916	1.81	9.7	4.1	0.825
Ma, Chan and Young (2015)	S700	H200×120×5	207	738	846	1.52	205	534	717	895	970	1.30	6.3	4.0	0.920
Wang, Zhao and Young (2020)	S960	A60×6-C	209	928	1012	2.45	202	748	899	1036	1171	2.40	9.8	3.9	0.800

Table 5. Different cases considered when corner material properties are available.

Cases	Availability of material parameters								
	E_c	$f_{0.01c}$	$f_{0.05c}$	f_{yc}	f_{uc}	ε_{uc}	n	m	m_{ma}
1	Known	Known	Known	Known	Known	Known	Known	Known	Known
2	Known	Eq. (24)	Eq. (25)	Known	Known	Eq. (23)	Eqs. (3) and (25)	Eq. (6)	Eq. (28)
3	197 GPa	Eq. (24)	Eq. (25)	Known	Eq. (19)	Eq. (23)	Eqs. (3) and (25)	Eq. (6)	Eq. (28)

Table 6. Predicted material parameters when corner material properties are available.

Specimen		E_c /GPa	f_{yc} /MPa	f_{uc} /MPa	$f_{0.01c}$ /MPa	$f_{0.05c}$ /MPa	ε_{uc} /%	n -	m -	m_{ma} -
235-5-90-10-3	Case 2	190	460	513	304	390	1.88	8.4	4.0	0.60
	Case 3	197	460	539	304	390	4.30	8.4	3.8	0.38
355-5cR-90-3-1	Case 2	185	613	681	376	503	1.82	7.0	4.0	0.62
	Case 3	197	613	683	376	503	1.70	7.0	4.0	0.60
460-3-120-P5-2	Case 2	187	610	664	375	501	1.53	7.0	4.0	0.72
	Case 3	197	610	680	375	501	2.04	7.0	4.0	0.60
CS-B4	Case 2	206	850	916	507	690	1.43	6.6	4.1	0.77
	Case 3	197	850	911	507	690	1.32	6.6	4.1	0.80
H200×120×5	Case 2	205	895	970	533	726	1.49	6.6	4.0	0.74
	Case 3	197	895	955	533	726	1.37	6.6	4.1	0.82
A60×6-C	Case 2	202	1036	1171	614	839	2.15	6.6	3.9	0.54
	Case 3	197	1036	1093	614	839	1.20	6.6	4.1	0.88

Table 7. Different cases considered when corner material properties are unavailable

Cases	Availability of material parameters												
	E_f	f_{yf}	f_{uf}	r_i/t	E_c	$f_{0.01c}$	$f_{0.05c}$	f_{yc}	f_{uc}	ε_{uc}	n	m	m_{ma}
4	Known	Known	Known	Known	$0.95E_f$	Eqs. (24) or (26)	Eqs. (25) or (27)	Eq. (17)	Eq. (18)	Eq. (23)	Eq. (3)	Eq. (6)	Eqs. (28) or (29)
5	-	Known	Eq. (30)	Known	197 GPa	Eqs. (24) or (26)	Eqs. (25) or (27)	Eq. (17)	Eq. (18)	Eq. (23)	Eq. (3)	Eq. (6)	Eqs. (28) or (29)

Table 8. Predicted material parameters when corner material properties are unavailable.

Specimen		f_{uf} /MPa	E_c /GPa	$f_{0.01c}$ /MPa	$f_{0.05c}$ /MPa	f_{yc} /MPa	f_{uc} /MPa	ε_{uc} /%	n -	m -	m_{ma} -
235-5-90-10-3	Case 4	464	200	298	373	450	519	2.66	7.4	3.9	0.45
	Case 5	450	197	291	369	443	508	2.49	7.6	3.9	0.47
355-5cR-90-3-1	Case 4	559	204	383	515	620	680	1.65	7.5	4.0	0.67
	Case 5	543	197	373	502	599	656	1.62	7.8	4.0	0.69
460-3-120-P5-2	Case 4	585	194	368	508	605	665	1.66	7.9	4.0	0.67
	Case 5	618	197	397	538	640	708	1.76	8.0	4.0	0.64
CS-B4	Case 4	837	206	497	708	856	934	1.58	7.3	4.0	0.70
	Case 5	866	197	525	738	888	974	1.64	7.5	4.0	0.68
H200×120×5	Case 4	846	197	558	755	892	976	1.61	8.3	4.0	0.69
	Case 5	813	197	530	721	849	926	1.56	8.5	4.0	0.71
A60×6-C	Case 4	1012	199	627	872	1043	1142	1.61	7.7	4.0	0.69
	Case 5	991	197	608	851	1019	1112	1.58	7.7	4.0	0.70